

LiBeam: Throughput-Optimal Cooperative Beamforming for Indoor Visible Light Networks

Nan Cen[†], Neil Dave[†], Emre Can Demirors[†], Zhangyu Guan[‡], Tommaso Melodia[†]

[†]Department of Electrical and Computer Engineering, Northeastern University, Boston, MA 02115

[‡]Department of Electrical Engineering, State University of New York (SUNY) at Buffalo, Buffalo, NY 14260

Email: {ncen, edemirors, melodia}@ece.neu.edu, dave.ne@husky.neu.edu, guan@buffalo.edu

Abstract—Indoor Visible Light Communications (VLC) are a promising technology to alleviate the looming spectrum crunch crisis in traditional RF spectrum bands. This article studies how to provide throughput-optimal WiFi-like downlink access to users in indoor visible light networks through a set of centrally-controlled and partially interfering light emitting diodes (LEDs). To reduce the effect of interference among users created by the partial overlap of each LED’s field of view, we propose LiBeam, a cooperative beamforming scheme, based on forming multiple LED clusters. Each cluster then serves a subset of users by jointly determining the user-LED association strategies and the beamforming vectors of the LEDs. The paper first proposes a mathematical model of the cooperative beamforming problem, presented as maximizing the sum throughput of all VLC users. Then, we solve the resulting mixed integer nonlinear nonconvex programming (MINCoP) problem by designing a globally optimal solution algorithm based on a combination of branch and bound framework as well as convex relaxation techniques. We then design for the first time a large programmable visible light networking testbed based on USRP X310 software-defined radios, and experimentally demonstrate the effectiveness of the proposed joint beamforming and association algorithm through extensive experiments. Performance evaluation results indicate that over 95% utility gain can be achieved compared to suboptimal network control strategies.

Index Terms—Visible Light Networking, Cooperative Beamforming, Throughput Optimization, Programmable Testbed.

I. INTRODUCTION

Indoor visible light communications (VLC) are a promising technology to alleviate the problem of an increasingly overcrowded RF spectrum, especially in unlicensed spectrum bands [1]–[5]. Unlike RF communications, VLC relies on a substantial portion of unregulated spectrum ranging from 375 THz to 750 THz, providing bandwidth orders of magnitude (10^4) wider than the available radio spectrum. In recent years, while there have been significant advances in understanding and designing efficient physical layer techniques (e.g., modulation schemes) [6] [7], the problem of designing optimized strategies to provide high-throughput WiFi-like access through VLC comms in indoor environments is still largely unexplored. To bridge this gap, in this article we focus on downlink indoor scenarios and study techniques to provide VLC-based wireless access to multiple concurrent users with optimized throughput using a set of centrally-controlled partially interfering LEDs.

There are multiple challenges to be addressed to provide high-throughput indoor visible light networking. First, VLC link quality is significantly affected by the imperfect, possibly time-varying, alignment between the communicating devices [8]. Hence, it is difficult to maintain reliable high-quality VLC links. Second, the link quality is degraded by the presence of mutual interference among adjacent partially interfering LEDs. Third, VLC links can easily get blocked because of the inherent low penetration of light. For these reasons, most existing work has focused either on link quality enhancement in single-link VLC systems [9] [10] or on the control of systems with multiple but non-coupled VLC links [11]–[13].¹ To address these challenges, in this paper we propose LiBeam, a new cooperative beamforming scheme for indoor visible light networking. In a nutshell, LiBeam uses multiple LEDs collaboratively to serve the same set of users thus reducing the interference among users and hence enhancing the quality of the visible light links.

Cooperative Visible Light Beamforming. VLC systems commonly exploit intensity modulation and direct detection (IM/DD), where an electrical signal is transformed into a real nonnegative waveform that carries *no phase information* to drive LEDs [1]. As a result, the conventional phase-shift-based RF beamforming techniques cannot be directly applied to VLC systems.

A few recent efforts have been made focused on VLC beamforming [13]–[15]. For example, Kim et al. propose in [14] time-division multiple access (TDMA) optical beamforming by using a specially-designed optical component, referred to as the spatial light modulator (SLM). In [15], the authors present a multiple-input-single-output (MISO) transmit beamforming system using a uniform circular array (UCA) as transmitter. Ling et al. propose a biased beamforming for multicarrier multi-LED VLC systems in [13]. However, these existing VLC beamforming techniques cannot be directly applied to indoor visible light downlink access networks, because (i) the existing lighting infrastructure is not easily modified by adding some special optical components or custom designed LEDs; (ii) existing beamforming schemes haven’t considered the interference among users, and hence are not suitable for indoor visible light networking with densely-deployed partially interfering LEDs.

In contrast to prior work, in this paper we propose a new

This work is based upon work supported in part by ONR grant N00014-17-1-2046 and NSF CNS-1618727.

¹We will discuss a few exceptions in Sec. II: Related Work.

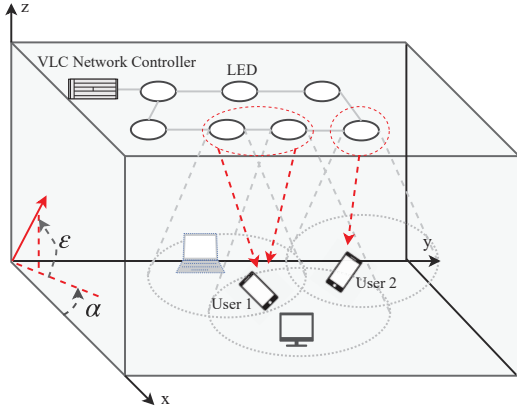


Fig. 1: Indoor visible light networking with cooperative beamforming.

beamforming technique to reduce the effects of interference among users in visible light networks using off-the-shelf LEDs. Specifically, our objective is to control the visible light signals so that they add constructively at the desired receiver if carrying the same information, and add destructively otherwise. Since it is difficult (if not impossible) to directly control the phase of the carrier signal (which is visible light here) as in traditional RF domain, we propose to control the beamforming weights (i.e., the amplitude and initial phase) of the *baseband electrical modulating signal*, and then use the resulting beamed electrical signal to modulate the visible light signal. Using aforementioned beamforming technique, we then propose LiBeam, a cooperative beamforming scheme for indoor visible-light downlink access network, as shown in Fig. 1, based on which the LEDs form multiple clusters, with each cluster serving a subset of the users by jointly determining the LED-user association strategies and the beamforming vectors of each LED cluster.

We claim the following main contributions:

- *Cooperative beamforming.* We formulate mathematically the cooperative beamforming problem with the control objective of maximizing the sum throughput of users in indoor visible-light downlink access networks, by jointly controlling the LED-user association and the beamforming vectors of the LEDs.
- *Globally-optimal solution algorithm.* To solve the resulting mixed integer nonlinear nonconvex programming (MINCoP) problem, we design a globally optimal solution algorithm based on a combination of the branch and bound framework and convex relaxation techniques.
- *Programmable visible light networking testbed.* We design for the first time a programmable indoor visible light networking testbed based on USRP X310 software-defined radios with a custom-designed optical front-end. The testbed consists of three main components: network control host, SDR control host, and VLC hardware and front-ends.
- *Experimental performance evaluation.* We experimentally demonstrate the effectiveness of the proposed cooperative beamforming scheme through extensive experiments.

The remainder of the paper is organized as follows. We review the related work in Section II, and then present the mathematical model of the cooperative beamforming scheme in Section III. The globally optimal solution algorithm is then described in Section IV. In Section V we discuss the design of the programmable visible-light networking testbed. Then, simulation and experimental performance evaluation results are presented in Section VI, and finally we draw main conclusions in Section VII.

II. RELATED WORK

There is a growing body of literature on visible light communications, mainly focusing on designing efficient physical layer techniques (e.g., modulation schemes) [9] [16] [17]. Recently, several results on visible light beamforming [11] [13]–[15] [18] and visible-light communication testbeds [19]–[22] have been presented. For example, [14] proposes a TDMA optical beamforming system based on a special optical component (SLM) to mechanically steer the light beams to the desired user. In [15], the authors propose a new indoor positioning system by adopting a uniform circular array (UCA) LEDs as transmitter to increase positioning accuracy. Ling et al. propose in [13] a beamforming scheme by jointly determining the DC bias of each LED and the beamforming vectors to maximize the sum throughput for OFDM multicarrier VLC system. In [18], a beamforming scheme is proposed to improve the secrecy performance under the assumption that there are multiple LED transmitters and one legitimate user. Most of these approaches are designed for specific application scenarios, without considering a network scenario with mutual interference introduced by multiple densely-deployed LEDs.

On the experimental front, a few platforms have been proposed in recent years for rapid prototyping of VLC communications. In [22], a software-defined single-link VLC platform utilizing WARP is presented. Gavrinca et al. prototype in [21] a USRP-platform-based visible light communication system based on the IEEE 802.15.7 standard. The authors of [19] and [20] present OpenVLC and the improved version OpenVLC1.0 based on Beagle-Bone Black (BBB) board, with the objective of being a starter kit for low-cost and low-data-rate VLC research. Most of these existing testbeds are focused on single-link demonstrations, where a networking perspective is not the core focus. To the best of our knowledge, no large-scale programmable indoor visible-light networking prototypes have been proposed so far.

III. SYSTEM MODEL AND PROBLEM FORMULATION

We consider an indoor visible light downlink access network scenario as illustrated in Fig. 1, where a set of LED transmitters form multiple clusters and in each cluster LEDs cooperatively transmit signal to the associated user. The set of LED transmitters is denoted as \mathcal{N} , with $|\mathcal{N}| = N$ being the number of LED transmitters, and the set of visible-light users is denoted as \mathcal{U} , with $|\mathcal{U}| = U$ representing the number of total users in the room. We assume that the LED transmitters are installed on the ceiling at pre-defined locations, straightly facing downwards. We also assume that the information of

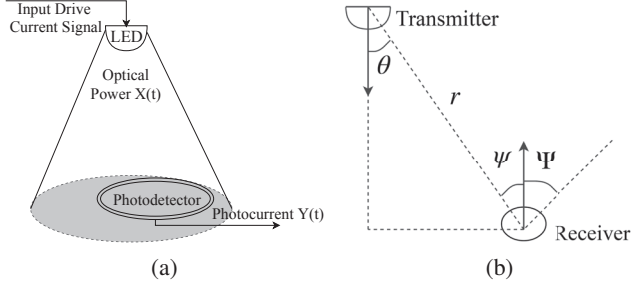


Fig. 2: (a) Transmission and reception in a visible light link with IM/DD, (b) Geometry LOS propagation model.

location, azimuth angle and elevation angle of the users can be obtained by the devices themselves [23]. As shown in Fig. 1, the azimuth angle (denoted as α) of a vector is the angle between the x -axis and the orthogonal projection of the vector onto the xy -plane. The elevation angle (denoted as ε) is the angle between the vector and its orthogonal projection onto the xy -plane.

IM/DD Channel. We consider an intensity modulation and direct detection (IM/DD) model, as illustrated in Fig. 2, which is often modeled as a baseband linear system [24] as

$$Y(t) = RX(t) \otimes h(t) + N(t), \quad (1)$$

where $X(t)$ and $Y(t)$ denote the instantaneous input power and the output current, respectively; R represents the detector responsivity; $N(t)$ is channel noise² and the symbol \otimes denotes the convolution operation. Unlike RF wireless channels, the frequency selectivity of the channel in VLC networks is mostly a consequence of hardware impairments of the transmit/receive devices (e.g., LEDs and PDs) rather than caused by the multipath nature of RF wireless channels. Moreover, the frequency selective characteristics of optical devices is substantially static and independent of the users' positions or orientations. However, the average received power is much more dynamic and is significantly dependent on the position and orientation of the user devices. Therefore, in this article, we assume that the visible-light channel is frequency non-selective, i.e.,

$$h(t) = H_0 \delta(t), \quad (2)$$

where $\delta(\cdot)$ is the dirac delta function and H_0 denotes the static gain of the impulse response of the visible-light gain and follows the Lambertian radiation pattern [26], given as

$$H_0 = \begin{cases} \frac{A(m+1)}{2\pi r^2} \cos^m(\theta) T_s(\psi) g(\psi) \cos(\psi) & 0 \leq \psi \leq \Psi, \\ 0 & \text{otherwise,} \end{cases} \quad (3)$$

where A is the physical area of the PD, and m is the Lambertian emission index and is given by the semi-angle $\psi_{1/2}$ at half illuminance power of an LED as $m = \frac{\ln 2}{\ln(\cos \psi_{1/2})}$. As illustrated in Fig. 2(b), r is the distance between a transmitter and a receiver, θ is the irradiance angle, ψ is the incidence angle, and Ψ denotes the field of view of PD. $T_s(\psi)$ and $g(\psi)$ represent the gain of an optical filter and the gain of an optical concentrator [26], respectively. Then, the channel model in (1) can be rewritten as

² $N(t)$ usually follows signal-independent additive Gaussian distribution [25].

$$Y(t) = RHX(t) + N(t). \quad (4)$$

Orientation- and Location-based Link Status. In visible-light networks, the field of views are limited for both LEDs and visible-light user receivers (i.e., photodetector (PD)). Therefore, LEDs and users may be out-of-FOV from each other, i.e., the transmit-receive link may not exist for some LED-user pairs. Therefore, determining the link status among LED-user pairs is the fundamental step in visible light networking. We denote the location and orientation information for the n -th LED transmitter as $P^n = [x^n, y^n, z^n, \alpha^n, \varepsilon^n]$, with $1 \leq n \leq N$. Accordingly, the location and orientation information for the j -th LED user is denoted as $P^u = [x^u, y^u, z^u, \alpha^u, \varepsilon^u]$, with $1 \leq u \leq U$. Since the LEDs are installed on the ceiling and straightly face downwards, the irradiance angle (denoted as θ_n^u) from n -th LED to u -th user can be calculated as

$$\theta_n^u = \text{atan2d}(\|\mathbf{V}_{-z} \times \mathbf{V}_u\|_2, \mathbf{V}_{-z}^T \mathbf{V}_u), \quad (5)$$

with $\mathbf{V}_{-z} = [0, 0, -1]^T$ being the unit norm vector of the n -th LED, $\mathbf{V}_u = [x^u, y^u, z^u]^T - [x^n, y^n, z^n]^T$ representing the vector that points to the u -th user from the n -th LED transmitter, and $\text{atan2d}(\cdot)$ is the function used to calculate the four-quadrant inverse tangent in degree [27]. Accordingly, the incidence angle ψ_u^n from n -th LED to the u -th user is calculated as

$$\psi_u^n = 90 - \text{atan2d}(\|\mathbf{V}_u \times \mathbf{V}_n\|_2, \mathbf{V}_u^T \mathbf{V}_n), \quad (6)$$

where \mathbf{V}_u is the unit vector of user, calculated based on the obtained orientation information of u -th user as $\mathbf{V}_u = [\cos(\alpha^u)\cos(\varepsilon^u), \sin(\alpha^u)\cos(\varepsilon^u), \cos(\varepsilon^u)]^T$, and $\mathbf{V}_n = [x^n, y^n, z^n]^T - [x^u, y^u, z^u]^T$ is the vector pointing to the n -th LED from the u -th user.

With θ_n^u and ψ_u^n , we then can determine if there exists a transmit-receive link between the n -th LED and the u -th user, as follows:

$$l_{n,u} = \begin{cases} 1, & \theta_n^u \leq \Theta, \psi_u^n \leq \Psi, \\ 0, & \text{Otherwise,} \end{cases} \quad (7)$$

with $l_{n,u}$ representing the link status between LED n and user y , and Θ and Ψ represent the FOV of LEDs and users, respectively. We denote $\mathbf{l} = \{l_{n,u} | 1 \leq n \leq N, 1 \leq u \leq U\}$ as the set of the link status between LEDs and users.

LED-User Association. In this article, we consider single-guest service for LED transmitters, i.e., each LED can serve at most one user in each cooperative transmission. Denote the LED-user association vector as $\boldsymbol{\mu} = \{\mu_{n,u} | n \in \mathcal{N}, u \in \mathcal{U}\}$, where $\mu_{n,u} = 1$ if LED n is selected to serve user u and a link exists between them, i.e., $l_{n,u} = 1$, and $\mu_{n,u} = 0$ otherwise. Then, we have

$$\mu_{n,u} \in \{0, 1\}, \forall n \in \mathcal{N}, \forall u \in \mathcal{U}, \quad (8)$$

$$\sum_{u \in \mathcal{U}} \mu_{n,u} = 1, \forall n \in \mathcal{N}, \quad (9)$$

$$\mathcal{N}_u \triangleq \{n | n \in \mathcal{N}, \mu_{n,u} = 1\}, \forall u \in \mathcal{U}, \quad (10)$$

$$\mathcal{N}_u^l \triangleq \{n | n \in \mathcal{N}, l_{n,u} = 1\}, \forall u \in \mathcal{U}. \quad (11)$$

Cooperative Transmission With Beamforming. Denote $d_{n,u}$ as the symbol to be transmitted to the u -th user from n -th LED. We assume $d_{n,u}$ is zero mean normalized to the range

$[-1, 1]$. At the n -th LED transmitter, to enable cooperative beamforming, $d_{n,u}$ is multiplied by beamforming weight $w_{n,u}$. Furthermore, to make the resulting input electrical signal positive, a bias B needs to be added to $d_{n,u}w_{n,u}$. Then, we obtain the input electrical signal from LED n to user u as

$$y_{n,u} = d_{n,u}w_{n,u} + B. \quad (12)$$

To ensure the nonnegativity of $y_{n,u}$, we need

$$|d_{n,u}w_{n,u}| \leq B, \forall n \in \mathcal{N}, \forall u \in \mathcal{U}. \quad (13)$$

In IM/DD visible-light system, the emitted light intensity is proportional to the input signal. Therefore, without loss of generality, we assume that the emitted light intensity equals the input signal and represented the same as in (12).

Light carrying signal propagates from the LED to the user where we only consider the line-of-sight (LOS) propagation path. The channel gain from the n -th LED to the u -th user is given by

$$h_{n,u} = \begin{cases} \frac{A_u(m+1)}{2\pi r_{n,u}^2} \cos^m(\theta_n^u) T_s(\psi_u^n) g(\psi_u^n) \cos(\psi_u^n) & 0 \leq \psi_u^n \leq \Psi, \\ 0 & \text{otherwise,} \end{cases} \quad (14)$$

where θ_n^u and ψ_u^n denote the incidence and irradiance angles between the n -th LED transmitter and user u , respectively, and $r_{n,u}$ represents the distance between the n -th transmitter and the u -th user.

Let $\mathbf{w}_u = [w_{1,u}, w_{2,u}, \dots, w_{N,u}]$ denote the beamforming vector for the u -th user, and $\mathbf{w} = [w_1, w_2, \dots, w_U]^T$ represent the beamforming weights matrix. Let $\mathbf{h}_u = [h_{1,u}, h_{2,u}, \dots, h_{N,u}]$ denote the channel gain vector for the u -th user, and $\mathbf{h} = [\mathbf{h}_1, \mathbf{h}_2, \dots, \mathbf{h}_U]^T$ represent the channel matrix. After removing the DC component at the PDs of the users, the received signal at the u -th user can be written as

$$\begin{aligned} r_u &= \sum_{n \in \mathcal{N}_u} d_{n,u} w_{n,u} h_{n,u} + \sum_{n \in (\mathcal{N}_u^l - \mathcal{N}_u)} d_{n,k} w_{n,k} h_{n,k} + z_u^2, \\ &= (\mathbf{h}_u^\mu)^T \mathbf{w}_u^\mu \mathbf{d}_u^\mu + (\mathbf{h}_u^l)^T \mathbf{w}_u^l \mathbf{d}_u^l + z_u, \end{aligned} \quad (15)$$

where the first term $(\mathbf{h}_u^\mu)^T \mathbf{w}_u^\mu \mathbf{d}_u^\mu$ is the desired signal, the second term $(\mathbf{h}_u^l)^T \mathbf{w}_u^l \mathbf{d}_u^l$ is the interference from other users, and z_u denotes the power of noise at user u . In VLC, z_u is considered to be Gaussian distributed with zero-mean and variance σ_u^2 [1]. The other symbols in (15) are defined as

$$\mathbf{h}_u^\mu = \boldsymbol{\mu}_u \circ \mathbf{h}_u, \forall u \in \mathcal{U}, \quad (16)$$

$$\mathbf{w}_u^\mu = \boldsymbol{\mu}_u \circ \mathbf{w}_u, \forall u \in \mathcal{U}, \quad (17)$$

$$\mathbf{d}_u^\mu = \boldsymbol{\mu}_u \circ \mathbf{d}_u, \forall u \in \mathcal{U}, \quad (18)$$

$$\mathbf{h}_u^l = (\mathbf{l}_u - \boldsymbol{\mu}_u) \circ \mathbf{h}_u, \forall u \in \mathcal{U}, \quad (19)$$

$$\mathbf{w}_u^l = (\mathbf{l}_u - \boldsymbol{\mu}_u) \circ \sum_{u \in \mathcal{U}} \mathbf{w}_u^\mu, \forall u \in \mathcal{U}, \quad (20)$$

$$\mathbf{d}_u^l = (\mathbf{l}_u - \boldsymbol{\mu}_u) \circ \sum_{u \in \mathcal{U}} \mathbf{d}_u^\mu, \forall u \in \mathcal{U}, \quad (21)$$

where \circ represents Hadamard product and $\mathbf{d}_u = [d_{1,u}, d_{2,u}, \dots, d_{N,u}]$ denotes the transmitted signal vector for the u -th user.

Signal-to-Interference-plus-Noise Ratio (SINR). In indoor visible-light networks, multiple transmissions usually

occur concurrently, thus introducing mutual interference at the receiver side. Therefore, the notion of SINR is adopted in this work to measure the signal quality at the user end. Denote γ_u as the SINR for user u , then it can be given as

$$\gamma_u = \frac{B^2 (\mathbf{h}_u^\mu)^T \mathbf{w}_u^\mu (\mathbf{w}_u^\mu)^T \mathbf{h}_u^\mu}{z_u + B^2 (\mathbf{h}_u^l)^T \mathbf{w}_u^l (\mathbf{w}_u^l)^T \mathbf{h}_u^l}. \quad (22)$$

Problem Statement. The network control objective can be stated as maximizing the sum utility of indoor visible-light downlink access network by jointly considering the position and orientation, FOVs of the LED transmitters and users, the LED-user association vectors, as well as the beamforming vectors for cooperative transmission and interference cancellation, subject to the following constraints:

- *Signal amplitude constraints:* To ensure the nonnegativity of the electrical signal input to the LEDs and to maintain linear current-to-light conversion, the amplitude of the transmitted signal is constrained as (13).
- *Beamforming weight coefficients:* To avoid violating the constraints of the modulated signal amplitude, when introducing beamforming weights, the following constraints should be satisfied:

$$|\mathbf{w}_u^\mu| \leq B, \quad (23)$$

$$|\mathbf{w}_u^l| \leq B. \quad (24)$$

Define $\mathbf{l} = \{l_{n,u} | n \in \mathcal{N}, u \in \mathcal{U}\}$ as the link status with respect to position, orientation and FOV of LEDs and users. Denote $\boldsymbol{\mu} = \{\mu_{n,u} | n \in \mathcal{N}, u \in \mathcal{U}\}$ and $\mathbf{w} = \{w_{n,u} | n \in \mathcal{N}, u \in \mathcal{U}\}$ as LED-user association and the beamforming vectors, respectively. Further define $\mathbf{P}_\mathcal{N} = [P^1, P^2, \dots, P^N]$ and $\mathbf{P}_\mathcal{U} = [P^1, P^2, \dots, P^U]$ as the location and orientation information of LEDs and users. The network control problem can then be formulated as

Problem 1: Given: $\Gamma, \mathbf{P}_\mathcal{N}, \mathbf{P}_\mathcal{U}, \Theta, \Psi, \mathbf{l}$

$$\text{Maximize}_{\boldsymbol{\mu}, \mathbf{w}} f = \sum_{u \in \mathcal{U}} R_u(\boldsymbol{\mu}, \mathbf{w}) \quad (25)$$

$$\text{Subject to: } (8), (9), (13), (16) \sim (21), (23), (24),$$

with $R_u = \log_2(1 + \gamma_u)$ representing the achievable throughput of user u .

IV. GLOBALLY OPTIMAL SOLUTION ALGORITHM

As stated in Sec. III, the *social* objective of the indoor multi-user visible-light network control problem is to maximize the sum throughput of the users by jointly controlling LED-user association strategies and the cooperative beamforming vectors, as presented in Problem 1. In (25), the individual SINR γ_u is a nonconvex function with respect to LED-user association vector $\boldsymbol{\mu}$ and the beamforming vectors \mathbf{w} . Moreover, the LED-user association variable $\boldsymbol{\mu}$ can only take binary values. Therefore, the resulting network control problem is a mixed nonlinear nonconvex programming (MINCoP) problem, for which there is in general no existing solution algorithm that can be used to obtain the global optimum in polynomial computational complexity. In this paper, we design a globally optimal solution algorithm based on a combination of the

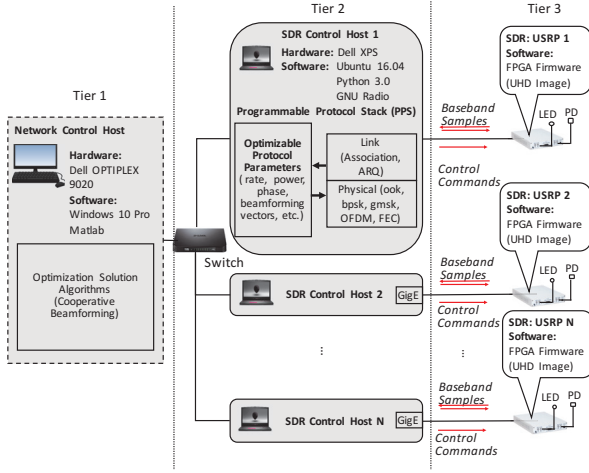


Fig. 3: Diagram of programmable visible light networking testbed.

branch and bound method and of convex relaxation techniques [28] [29].

A. Overview of The Algorithm

The objective of the proposed algorithm is to solve the MINCoP formulated in Problem 1 by exploiting branch-and-bound framework [30]. With this approach, we aim to search for an ϵ -optimal solution, with $\epsilon \in (0, 1]$ being the predefined optimality precision that can be set as close to 1 as we wish. Denote $\mathcal{Q}_0 = \{\boldsymbol{\mu}, \boldsymbol{w} \mid \text{constraints in (25)}\}$ as the feasible set of the initial problem (25), and $U^*(\mathcal{Q}_0)$ as the global optimum of problem (25) over \mathcal{Q}_0 , then our objective is to search iteratively for U so that $U(\mathcal{Q}_0) \geq \epsilon U^*(\mathcal{Q}_0)$.

To this end, the algorithm maintains a set $\mathcal{Q} = \{\mathcal{Q}_i, i = 0, 1, 2, \dots\}$ of subproblems by iteratively partitioning feasible set \mathcal{Q}_0 into a series of smaller subsets \mathcal{Q}_i . During the iterations, the algorithm also maintains a global upper bound $\bar{U}_{\text{glb}}(\mathcal{Q}_0)$ and a global lower bound $\underline{U}_{\text{glb}}(\mathcal{Q}_0)$ on $U^*(\mathcal{Q}_0)$ so that

$$\underline{U}_{\text{glb}}(\mathcal{Q}_0) \leq U^*(\mathcal{Q}_0) \leq \bar{U}_{\text{glb}}(\mathcal{Q}_0). \quad (26)$$

The global upper and lower bounds are updated as follows:

$$\bar{U}_{\text{glb}}(\mathcal{Q}_0) = \max\{\bar{U}_{\text{glb}}(\mathcal{Q}_i), i = 1, 2, \dots\}, \quad (27)$$

$$\underline{U}_{\text{glb}}(\mathcal{Q}_0) = \max\{\underline{U}_{\text{glb}}(\mathcal{Q}_i), i = 1, 2, \dots\}. \quad (28)$$

Then, if $\underline{U}_{\text{glb}}(\mathcal{Q}_0) \geq \epsilon \bar{U}_{\text{glb}}(\mathcal{Q}_0)$, it indicates that the predefined optimality precision ϵ is achieved, and then the algorithm terminates and sets the optimal sum rate to $U^*(\mathcal{Q}_0) = \underline{U}_{\text{glb}}(\mathcal{Q}_0)$. Otherwise, the algorithm chooses a sub-domain from \mathcal{Q} and partition it into two sub-domains. In our algorithm, we select sub-domain \mathcal{Q}_i with the highest local upper bound, i.e., $i = \text{argmax}_i \bar{U}_{\text{glb}}(\mathcal{Q}_i)$. Based on the global bounds update criterion in (27) and (28), the gap between the two global bounds converges to 0 as the partition progresses. Furthermore, from (26), $\underline{U}_{\text{glb}}(\mathcal{Q}_0)$ and $\bar{U}_{\text{glb}}(\mathcal{Q}_0)$ converge to the global optimum $U^*(\mathcal{Q}_0)$.

B. Convex Relaxation

Because the problem formulated in Sec. III is nonconvex, a key step in the algorithm described above is to obtain a relaxed but convex version of the original problem (25) and

the subproblems resulting from the partition, so that a tight local upper bound $\bar{U}_{\text{glb}}(\mathcal{Q}_i)$ can be easily computed for each of them. To this end, we first relax the LED-user association variables $\mu_{n,u}$, $n \in \mathcal{N}$, $u \in \mathcal{U}$ in (25), which take binary values only, by allowing each LED to serve multiple user nodes. Then the constraint in (8) can be rewritten as

$$0 \leq \mu_{n,u} \leq 1 \quad \forall n \in \mathcal{N}, \forall u \in \mathcal{U}, \quad (29)$$

and the individual throughput R_u in problem (25) can be further expressed as

$$R_u = \log_2(1 + \gamma_u) \quad (30)$$

$$= \log_2\left(1 + \frac{B^2(\mathbf{h}_u^\mu)^T \mathbf{w}_u^\mu (\mathbf{w}_u^\mu)^T \mathbf{h}_u^\mu}{z_u + B^2(\mathbf{h}_u^l)^T \mathbf{w}_u^l (\mathbf{w}_u^l)^T \mathbf{h}_u^l}\right) \quad (31)$$

$$= \log_2\left(\frac{z_u + B^2(\mathbf{h}_u^\mu)^T \mathbf{w}_u^\mu (\mathbf{w}_u^\mu)^T \mathbf{h}_u^\mu}{z_u + B^2(\mathbf{h}_u^l)^T \mathbf{w}_u^l (\mathbf{w}_u^l)^T \mathbf{h}_u^l}\right) \quad (32)$$

$$= \log_2(z_u + B^2(\mathbf{h}_u^l)^T \mathbf{w}_u^l (\mathbf{w}_u^l)^T \mathbf{h}_u^l + B^2(\mathbf{h}_u^\mu)^T \mathbf{w}_u^\mu (\mathbf{w}_u^\mu)^T \mathbf{h}_u^\mu) \quad (33)$$

$$- \log_2(z_u + B^2(\mathbf{h}_u^l)^T \mathbf{w}_u^l (\mathbf{w}_u^l)^T \mathbf{h}_u^l), \quad (34)$$

According to composition rule (i.e., composition operations preserve convexity) in convex optimization [31], the first and second parts (including the minus sign) in (30) are convex and concave, respectively. Therefore, a convex relaxation of (30) can be obtained by approximating the logarithm operation in the concave part of (30) using a set of linear functions. To this end, we first replace $z_u + B^2(\mathbf{h}_u^l)^T \mathbf{w}_u^l (\mathbf{w}_u^l)^T \mathbf{h}_u^l$ in the second part of (30) with t , then $\log_2(z_u + B^2(\mathbf{h}_u^l)^T \mathbf{w}_u^l (\mathbf{w}_u^l)^T \mathbf{h}_u^l)$ in (30) can be represented as $\log_2(t)$ subject to $t \geq (z_u + B^2(\mathbf{h}_u^l)^T \mathbf{w}_u^l (\mathbf{w}_u^l)^T \mathbf{h}_u^l)$. Then $\log_2(t)$ can be further relaxed using a segment and three tangent lines [31].

Then the original MINCoP problem in (25) can be reformulated as a convex problem as

Problem 2: Given: $\Gamma, \mathbf{P}_{\mathcal{N}}, \mathbf{P}_{\mathcal{U}}, \Theta, \Psi, \mathbf{l}$

$$\text{Maximize}_{\boldsymbol{\mu}, \boldsymbol{w}} f = \sum_{u \in \mathcal{U}} R_{ua}(\boldsymbol{\mu}, \boldsymbol{w}), \quad (35)$$

$$\text{Subject to: (9), (13), (16) } \sim \text{(21), (23), (24), (29)}$$

with R_{ua} representing the relaxed convex version of R_u in (25). As variable partition progresses, the association variable $\mu_{n,u}$ becomes fixed to either 0 or 1 in all subproblems, for which the optimal beamforming weights \boldsymbol{w} can be obtained by solving a convex programming problem (35).

C. Variable Partition

Variable partition can be conducted by partitioning association variable $\boldsymbol{\mu}$ and the beamforming variables \boldsymbol{w} . For example, given a subproblem \mathcal{Q}_i , by fixing association variable $\mu_{n,u}$ subproblem \mathcal{Q}_i can be partitioned into two subproblems with feasible set $\mathcal{Q}_{i,1} = \{(\boldsymbol{\mu}, \boldsymbol{w}) \in \mathcal{Q}_i \mid \mu_{n,u} = 0\}$ and $\mathcal{Q}_{i,2} = \{(\boldsymbol{\mu}, \boldsymbol{w}) \in \mathcal{Q}_i \mid \mu_{n,u} = 1\}$, respectively. For the beamforming vectors, say $w_{n,u} \in [w_{n,u}^{\min}, w_{n,u}^{\max}]$ for LED n to user u , the partition can be conducted by splitting $w_{n,u}$ from the half, resulting in two subproblems with feasible sets

$$\mathcal{Q}_{i,1} = \{(\boldsymbol{u}, \boldsymbol{w}) \in \mathcal{Q}_i \mid w_{n,u} \in [w_{n,u}^{\min}, w_{n,u}^{\text{mid}}]\}, \quad (36)$$

$$\mathcal{Q}_{i,2} = \{(\boldsymbol{u}, \boldsymbol{w}) \in \mathcal{Q}_i \mid w_{n,u} \in [w_{n,u}^{\text{mid}}, w_{n,u}^{\max}]\}, \quad (37)$$

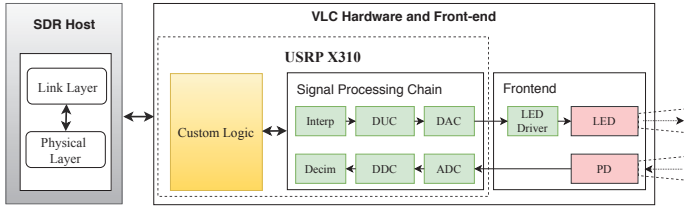


Fig. 4: Architecture of a software-defined visible-light node.

where $w_{n,u}^{mid} \triangleq \frac{w_{n,u}^{min} + w_{n,u}^{max}}{2}$.

V. TESTBED DEVELOPMENT

As discussed in Sec. II, most of existing visible-light testbeds are focused on single-link implementation. To the best of our knowledge, we design for the first-time a large programmable indoor visible-light networking prototype, which can support arbitrary N nodes.

Overall Diagram. The prototyping diagram is illustrated in Fig. 3, following a hierarchical architecture with three tiers, i.e., network control host, SDR control host and VLC hardware and front-ends. At the top tier of the hierarchical architecture is the network control host, where the designed optimization solution algorithms are executed. The output of this tier is a set of optimal variables, which will then be sent to each of the SDR control hosts. At the second tier, the programmable protocol stack (PPS) is installed on each of the SDR control hosts. With the optimal variables received from the network control host, the PPS will be compiled to generate operational code to control at network run time the VLC hardware and front-ends of the third tier. Finally, each of the VLC hardware and front-ends (i.e., USRP) receives the baseband samples from its control host via Gigabit Ethernet (GigE) interface and then sends them over the air with transmission parameters specified in the control commands from the SDR control hosts.

Network Control Host. The network control host is a Dell OPTIPLEX 9020 desktop running Windows 10 pro. On the host the networking optimization algorithms designed in Sec. IV are executed to solve the cooperative beamforming problem formulated in (25). The output of the algorithms is the optimized LED-user association vector and beamforming vectors.

SDR Control Host. As shown in Fig. 3, the programmable protocol stack (PPS) is installed on each of the SDR control hosts, which are Dell XPS running Ubuntu 16.04. The PPS has been developed in Python on top of GNU Radio to provide seamless controls of USRPs. The developed PPS covers PHY and link layers currently, and can be easily extended to upper layers in future. As illustrated in Fig. 4, the architecture of the LiBeam node has been developed based on PPS to verify the effectiveness of the designed visible-light networking prototype. At the physical layer, a wide set of modulation schemes can be supported, including On-Off Keying (OOK), Gaussian minimum-shift keying (GMSK), binary phase-shift keying (BPSK), among others. The programmable parameters at this layer include modulation schemes, transmission power, and beamforming weights, among others. At the

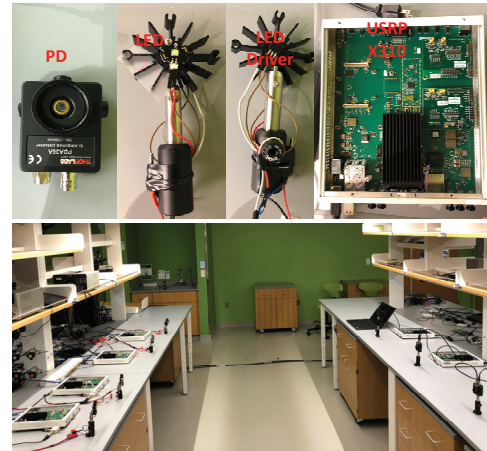


Fig. 5: Hardware components of visible-light node and a snapshot of the LiBeam testbed.

link layer, besides fragmentation/defragmentation, network-to-physical address translation, reliable point-to-point frame delivery, cooperative transmitter access control and LED cluster formation are particularly designed for LiBeam.

VLC Hardware and Front-ends. The hardware components of each LiBeam node and the snapshot of the LiBeam testbed are illustrated in Fig. 5. The LiBeam testbed is designed based on USRP X310 software-defined radios. The motherboard of each USRP X310 has four wideband daughterboard slots that support bandwidth of up to 120 MHz within DC - 6 GHz frequency. We currently use two slots of the motherboard to accommodate LFTX and LFRX daughterboards for visible light signal transmission and reception, while the remaining two slots are reserved for future extension, for example, RF/VLC coexistence prototype, MIMO VLC implementation.

At the transmitter side, we use a Bivar L2-MLW1-F LED with 125° field of view (FOV). We build an transconductance amplifier based LED driver from scratch to drive the LED, which mainly consists of a bias-T and a RF NPN transistor. The bias-T is used to combined the modulated AC waveform from USRP X310 and the DC bias that meets the minimum voltage requirement to light up the LED.

At the receiver side, we use Thorlabs PDA36A with FOV 90° , which can detect light with wavelength ranging from 350 to 1100 nm. PDA36A features a built-in low-noise transimpedance amplifier (TIA) with switchable gain and it can support bandwidth from DC to 12 MHz. The PDA36A consequently converts the received photons into real-valued digital samples and then sends them to the SDR control host for post-processing.

VI. PERFORMANCE EVALUATION

In this section, we first evaluate the proposed solution algorithm through simulations, and then we further validate experimentally the effectiveness of LiBeam over the designed prototype through testbed experiments.

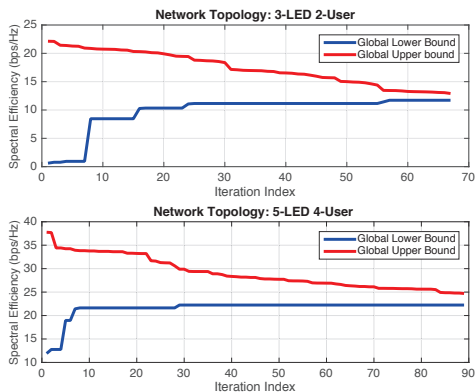


Fig. 6: Global upper and lower bounds of the globally optimal solution algorithm for network topology with (a) 3 LEDs and 2 users and (b) 5 LEDs and 4 users.

A. Simulation Results

We first evaluate the performance of the solution algorithm proposed in Sec. IV by considering an indoor area of $5 \times 5 \times 5$ m³, where $N = \{3, 4, \dots, 9\}$ LEDs serve $U = \{2, 3, 4, 5\}$ visible-light users. The altitude of the LEDs are set to 5 meters, emulating scenarios where all LEDs are mounted on the ceiling, straightly facing downwards. The FOVs of LED and user PD are both set to $2/3\pi$. The PD's physical area and responsivity are 10^{-5} m² and 0.5 A/W, respectively. The average noise power is set to $6.4640e^{-17}$ W. Results are obtained by randomly generating network topologies with a given number of LEDs and users, i.e., positions of LEDs, positions and orientations of users.

Figure 6 shows the convergence of the proposed solution algorithm with 3-LED 2-user and 5-LED 2-user scenarios. It can be seen that the proposed algorithm can converge very fast to the global optimum of the MINCoP problem formulated in (25), in around 70 and 90 iterations in Figs. 6(a) and (b), respectively.

In Fig. 7, we then compare the performance with respect to the network spectral efficiency of the proposed solution algorithm (aka, *Joint Optimization*) with other two strategies, i.e., *w/o Association* and *Greedy*. In *w/o Association*, the LED-user association is randomly generated. And in *Greedy*, the LED-user association is determined according to the best channel gain rule and the selected LED transmitting with maximum power. It can be seen that the joint network control achieves the highest spectral efficiency in almost all of the tested network topologies. When the randomly generated LED-user association of *w/o Association* strategy is occasionally the same as the *Joint Optimization* scheme, they will achieve the same network spectral efficiency. Results also show that when the LED-user association generated by *Greedy* is better than that of *w/o Association*, *Greedy* can slightly outperform *w/o association*, for example in network topology instance 13. To make the result clearer, Fig. 8 shows the increase of the network spectrum efficiency achievable by *Joint Optimization* compared to *w/o Association* and *Greedy*. We can clearly see that the proposed *Joint Optimization* algorithm outperforms

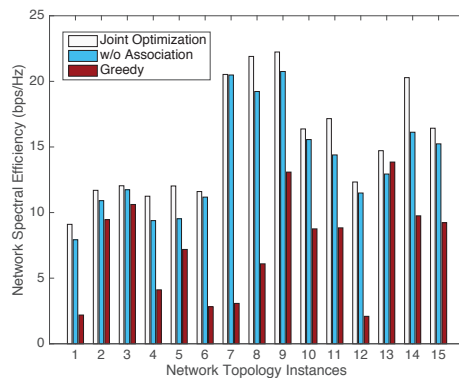


Fig. 7: Achievable network spectral efficiency with different network control strategies.

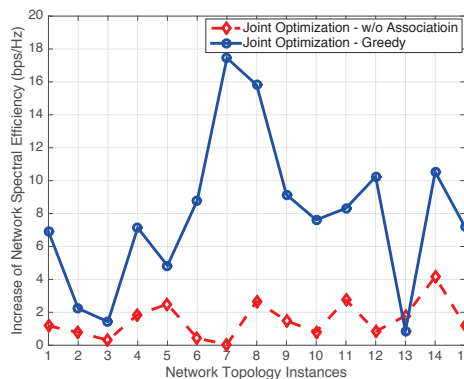


Fig. 8: Increase of network spectrum efficiency with different network control strategies.

the other two strategies, particularly the *Greedy* strategy.

B. Experimental Evaluation

As shown in Fig. 5, we set up the experimental testbed by using the software-defined programmable visible light networking node introduced in Sec. V to validate the proposed cooperative beamforming solution algorithm in indoor visible light networks. We designed two different networking scenarios (i.e., 4 LEDs 2 users and 4 LEDs 3 users) as shown in Tables I and II, respectively. In each network scenario, two different user position sets are used, where users in the first set are more densely deployed than in the second set. Without loss of generality, users' PDs straightly face towards the plain where LEDs located, with the azimuth and elevation angles being $\varepsilon = 90^\circ$ and $\alpha = 90^\circ$, respectively. Due to the limited bandwidth of the LED, 40 kHz bandwidth is set for each USRP. After modulation, the data is sampled at sampling rate of 800 kHz. The communication range in the experiments is set to 5 m. According to the specifications of the hardware components used in the experiments, the FOVs of LED and PD are 125° and 90° , respectively. The PD's active physical area is 1.3×10^{-5} m².

Before conducting the experiments, we first test the visible-light instantaneous channel response by using GoldSequence preamble. The results are shown in Fig. 9 obtained by sending 10000 preambles. We can see that the visible-light channel is

TABLE I: Network Scenario 1

Number Index	1	2	3	4
LED position (m)	(5, 0, 0)	(5, 1, 0)	(5, 1.5, 0)	(5, 3, 0)
User position 1 (m)	(3, 1, 0)	(3, 3.5, 0)		
User position 2 (m)	(3, 1, 0)	(3, 2, 0)		

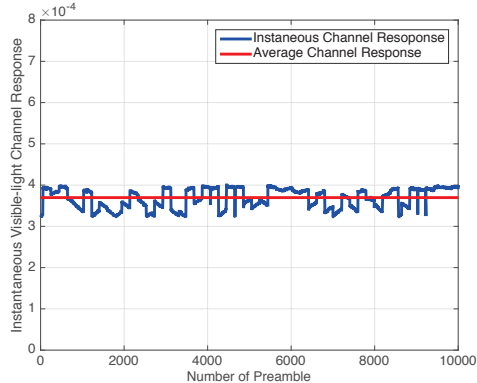


Fig. 9: Instantaneous visible-light channel response.

almost stable once the position of the LED and user as well as the corresponding optical parameters (e.g., PD active area, orientations of LEDs and PDs) are fixed, which is also satisfied the channel model presented in Sec. III.

We then test the effectiveness of the proposed *Joint Optimization* algorithm in terms of sum utility, by comparing it to the other two suboptimal network control strategies: *w/o Association* and *Greedy* algorithms. Figures 10 and 11 report the average end-to-end throughput (in terms of packets/s) achievable in the two tested network scenarios. The packet length in the experiments is set to 1500 bits. We observe that the proposed joint optimization method outperforms the other two methods in most of the tested instances, and up to 95.9% sum utility gain can be achieved in network scenario 2. In Fig. 10, for the second user position set, *Joint Optimization* achieves the same performance as *w/o Association*. This is because the *w/o Association* method may randomly select the same LED-user association as *Joint Optimization*. Figures 10 and 11 also show that more-densely-deployed users would suffer from severer mutual interference, resulting in lower average sum utility compared to the cases where users are deployed farther away from each other, especially with the *Greedy* method. This is because, with the *Greedy* algorithm, the transmitter with the best channel gain will be selected with the maximum power to transmit data to the desired user, thus resulting in higher interference to other users, especially when users are closer to each other. As a result, no packet can be successfully delivered with the *Greedy* method in the second test instance in of the two network scenarios.

Figure 12 provides a closer look at the contrasting behaviors in terms of the corresponding instantaneous throughput resulting from *Joint Optimization*, *w/o Association* and *Greedy* for the first user position set in network scenarios 1 and 2, respectively. It can be seen from Figs. 12(a) and (b) that, the instantaneous throughput obtained from these three methods are stable at some level, without or with little fluctuations only. These results are consistent with the observations in

TABLE II: Network Scenario 2

Number Index	1	2	3	4
LED position (m)	(5, 0, 0)	(5, 1, 0)	(5, 3, 0)	(5, 5, 0)
User position 1 (m)	(3, 1, 0)	(3, 3.5, 0)	(3, 5, 0)	
User position 2 (m)	(3, 0, 0)	(3, 1, 0)	(3, 2, 0)	

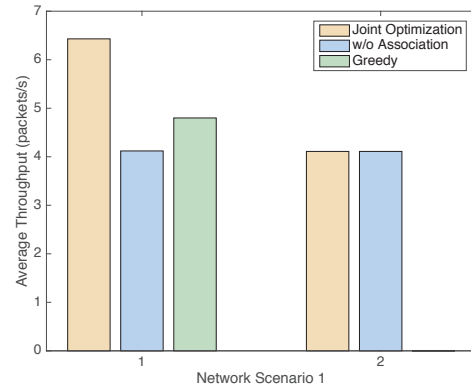


Fig. 10: Average sum utility of network scenario 1.

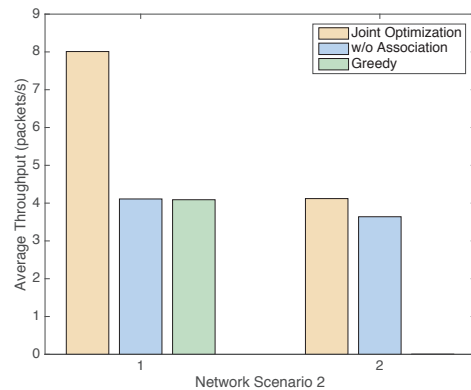


Fig. 11: Average sum utility of network scenario 2.

Fig. 9, where the instantaneous channel response is almost stable. We can also see that the proposed *Joint Optimization* method always outperforms the other two methods in terms of instantaneous throughput in real-time running experiments.

VII. CONCLUSIONS

We have proposed LiBeam, a new cooperative beamforming approach for indoor visible light networks with the objective of maximizing the sum throughput of the VLC users by jointly determining the user-LED association strategies and the beamforming vectors of the LEDs. We mathematically formulated the cooperative beamforming problem and a globally optimal solution algorithm has been designed to solve the problem. A programmable visible light networking testbed has also been developed, on which the effectiveness of the proposed LiBeam was validated through extensive simulation as well as experimental performance evaluation.

REFERENCES

- [1] T. Komine and M. Nakagawa, "Fundamental Analysis for Visible-light Communication System Using LED Lights," *IEEE Trans. on Consumer Electronics*, vol. 50, no. 1, pp. 100–107, February 2004.

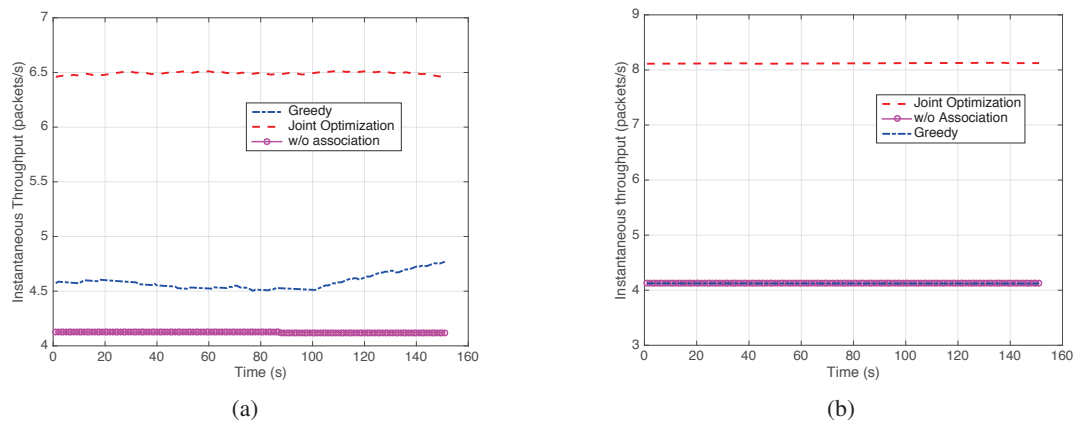


Fig. 12: Instantaneous throughput comparison for the first user position set of (a) network scenario 1 and (b) network scenario 2.

- [2] N. Cen, J. Jagannath, S. Moretti, Z. Guan, and T. Melodia, "LANET: Visible-Light Ad Hoc Networks," *Ad Hoc Networks (Elsevier)*, vol. 84, pp. 107–123, 2018.
- [3] P. Pathak, X. Feng, P. Hu, and P. Mohapatra, "Visible Light Communication, Networking and Sensing: A Survey, Potential and Challenges," *IEEE Communications Surveys Tutorials*, vol. 17, no. 4, pp. 2047–2077, Fourthquarter 2015.
- [4] S. Ucar, S. Coleri Ergen, O. Ozkasap, D. Tsonev, and H. Burchardt, "SecVLC: Secure Visible Light Communication for Military Vehicular Networks," in *Proc. of Intl. Symp. on Mobility Management and Wireless Access (MobiWac)*, Malta, November 2016.
- [5] H. Zhao, Y. Liu, K. Huang, X. Ji, and D. Wang, "A Study on Networking Scheme of Indoor Visible Light Communication Networks," in *Proc. of IEEE Vehicular Technology Conference (VTC)*, Seoul, South Korea, May 2014.
- [6] C. Chen, M. Ijaz, D. Tsonev, and H. Haas, "Analysis of downlink transmission in DCO-OFDM-based optical attocell networks," in *Proc. of IEEE Global Communications Conference (GLOBECOM)*, Austin, TX, Dec 2014.
- [7] Y. Wang, X. Huang, L. Tao, J. Shi, and N. Chi, "4.5-Gb/s RGB-LED based WDM Visible Light Communication System Employing CAP Modulation and RLS based Adaptive Equalization," *Optics Express*, vol. 23, no. 10, pp. 13 626–13 633, May 2015.
- [8] J. Zhang, X. Zhang, and G. Wu, "Dancing with Light: Predictive In-frame Rate Selection for Visible Light Networks," in *Proc. of IEEE Conf. on Computer Communications (INFOCOM)*, Hong Kong S.A.R., PRC, April 2015.
- [9] D. Tsonev, H. Chun, S. Rajbhandari, J. McKendry, S. Videv, E. Gu, M. Haji, S. Watson, A. Kelly, G. Faulkner, M. Dawson, H. Haas, and D. O'Brien, "A 3-Gb/s Single-LED OFDM-Based Wireless VLC Link Using a Gallium Nitride μ LED," *IEEE Photonics Technology Letters*, vol. 26, no. 7, pp. 637–640, April 2014.
- [10] C.-L. Chan, H.-M. Tsai, and K. C.-J. Lin, "POLI: Long-Range Visible Light Communications Using Polarized Light Intensity Modulation," in *Proc. of ACM International Conference on Mobile Systems, Applications, and Services (MobiSys)*, New York, USA, June 2017.
- [11] Z. Yu, R. J. Baxley, and G. T. Zhou, "Multi-user MISO Broadcasting for Indoor Visible Light Communication," in *Proc. of IEEE International Conference on Acoustics, Speech and Signal Processing*, Vancouver, Canada, May 2013.
- [12] L. Wang, C. Wang, X. Chi, L. Zhao, and X. Dong, "Optimizing SNR for Indoor Visible Light Communication via Selecting Communicating LEDs," *Optics Communications*, vol. 387, pp. 174 – 181, 2017.
- [13] X. Ling, J. Wang, X. Liang, Z. Ding, C. Zhao, and X. Gao, "Biased Multi-LED Beamforming for Multicarrier Visible Light Communications," *IEEE Journal on Selected Areas in Communications*, vol. 36, no. 1, pp. 106–120, January 2018.
- [14] S.-M. Kim, M.-W. Baek, and S. H. Nahm, "Visible Light Communication Using TDMA Optical Beamforming," *EURASIP Journal on Wireless Communications and Networking*, vol. 2017, no. 1, p. 56, March 2017.
- [15] N. Fujimoto and H. Mochizuki, "477 Mbit/s Visible Light Transmission based on OOK-NRZ Modulation Using a Single Commercially Available Visible LED and a Practical LED Driver with a Pre-emphasis Circuit," in *Proc. of IEEE Optical Fiber Communication Conference and Exposition and the National Fiber Optic Engineers Conference (OFC/NFOEC)*, Anaheim, CA, March 2013.
- [16] J. Armstrong and B. Schmidt, "Comparison of Asymmetrically Clipped Optical OFDM and DC-Biased Optical OFDM in AWGN," *IEEE Communications Letters*, vol. 12, no. 5, pp. 343–345, May 2008.
- [17] S. Cho, G. Chen, and J. P. Coon, "Securing Visible Light Communication Systems by Beamforming in the Presence of Randomly Distributed Eavesdroppers," *IEEE Transactions on Wireless Communications*, vol. 17, no. 5, pp. 2918–2931, May 2018.
- [18] Q. Wang, D. Giustiniano, and D. Puccinelli, "OpenVLC: Software-defined Visible Light Embedded Networks," in *Proc. of ACM MobiCom Workshop on Visible Light Communication Systems (VLCS)*, Maui, Hawaii, September, 2014.
- [19] Q. Wang, D. Giustiniano, and O. Gnawali, "Low-Cost, Flexible and Open Platform for Visible Light Communication Networks," in *Proc. of ACM International Workshop on Hot Topics in Wireless*, Paris, France, September 2015.
- [20] C. Gavrinca, J. Baranda, and P. Henarejos, "Rapid Prototyping of Standard-Compliant Visible Light Communications System," *IEEE Communications Magazine*, vol. 52, no. 7, pp. 80–87, July 2014.
- [21] Y. Qiao, H. Haas, and K. Edward, "Demo: A Software-defined Visible Light Communications System with WARP," in *Proc. of ACM MobiCom Workshop on Visible Light Communication Systems (VLCS)*, Maui, Hawaii, September, 2014.
- [22] T. Platform. [https://en.wikipedia.org/wiki/Tango_\(platform\)](https://en.wikipedia.org/wiki/Tango_(platform)).
- [23] J. M. Kahn and J. R. Barry, "Wireless Infrared Communications," *Proceedings of the IEEE*, vol. 85, no. 2, pp. 265–298, February 1997.
- [24] F. Miramirkhani and M. Uysal, "Channel Modeling and Characterization for Visible Light Communications," *IEEE Photonics Journal*, vol. 7, no. 6, pp. 1–16, Dec 2015.
- [25] Z. Ghassemlooy, W. Popoola, and S. Rajbhandari, *Optical Wireless Communications: System and Channel Modelling with MATLAB*. Boca Raton, FL, USA: CRC Press, Inc., 2012.
- [26] 2-Argument Arctangent. <https://en.wikipedia.org/wiki/Atan2>.
- [27] E. L. Lawler and D. E. Wood, "Branch-And-Bound Methods: A Survey," *Operations Research*, vol. 14, no. 4, pp. 699–719, Jul.-Aug. 1966.
- [28] H. D. Sherali and W. P. Adams, *A Reformulation-Linearization Technique for Solving Discrete and Continuous Nonconvex Problems*. Boston: MA: Kluwer Academic, 1999.
- [29] S. Boyd and J. M. Whinston, "Branch and Bound Methods," *Notes for EE364b, Stanford University*, Mar. 2007.
- [30] S. Boyd and L. Vandenberghe, *Convex Optimization*. Cambridge University Press, 2004.